

Current induced transverse spin-wave instability in thin ferromagnets: beyond linear stability analysis

Shaffique Adam, Mikhail L. Polianski,* and Piet W. Brouwer

Laboratory of Atomic and Solid State Physics, Cornell University, Ithaca, NY 14853-2501

(Dated: September 10, 2018)

A sufficiently large unpolarized current can cause a spin-wave instability in thin nanomagnets with asymmetric contacts. The dynamics beyond the instability is understood in the perturbative regime of small spin-wave amplitudes, as well as by numerically solving a discretized model. In the absence of an applied magnetic field, our numerical simulations reveal a hierarchy of instabilities, leading to chaotic magnetization dynamics for the largest current densities we consider.

PACS numbers: 75.75.+a, 75.40.Gb, 85.75.-d

I. INTRODUCTION

Almost a decade ago Slonczewski¹ and Berger² predicted that when a spin-polarized current is passed through a ferromagnet it transfers the transverse component of its spin angular momentum to the ferromagnet. The experimental verification of the theoretical predictions followed within a few years.^{3,4,5,6,7} Since then, the so-called ‘spin-transfer effect’ has been observed in a large number of different experiments.

In most experiments, the spin-transfer torque is studied in a ferromagnet–normal-metal–ferromagnet tri-layer structure where a thick ferromagnet first polarizes the current which then exerts a spin-transfer torque on a second thinner ferromagnet. At sufficiently large applied current densities, the spin-transfer torque then may alter the magnetization direction of the thin magnet. The observation of hysteretic magnetic switching for one current direction only was seen as a hallmark of the spin-torque effect,⁶ and excluded an explanation of the experiments in terms of the Faraday field associated with the applied current. (Note that for small system sizes, the spin-transfer torque, which scales proportional to the current density, dominates over the torque exerted by the magnetic field caused by the current flow, which is proportional to the total current.) Dynamical aspects of the magnetic switching process were addressed in recent experiments.^{8,9,10,11}

Over the past few years there has been much theoretical interest in understanding the spin-transfer torque and its consequences for hybrid ferromagnet–normal-metal devices. The connection between spin currents or spin accumulation in the normal metal spacer layer and the spin torque can be considered understood^{12,13,14} (see Ref. 15 for a recent review). Most calculations of the response of the magnetization to the spin-transfer torque have been done in the so-called ‘macrospin approximation’, assuming that the ferromagnets remain single domains dur-

ing spin-transfer induced switching events.^{16,17,18,19,20,21} They have addressed the precise nature of the magnetic switching process, the possibility of limit cycles, and the temperature dependence of the spin-transfer torque. In addition, full micromagnetic simulations have been done by several groups,^{22,23,24,25} *e.g.*, to examine the effect of the Ampere field on the hysteretic switching or the breakdown of the macrospin model into quasi-chaotic dynamics at very high current densities. While the micromagnetic simulations are a significant improvement on the macrospin approximation when it comes accounting for spatial non-uniformities in the switching process, the existing simulations derive the spin-transfer torque from an externally fixed spin current, which is a poor description of the experimental geometries in which the spin currents are determined as an intricate combination of spin polarizations caused by all ferromagnetic elements in the device.^{12,15,26,27}

In a recent work, two of the authors showed that a sufficiently large but unpolarized electrical current flowing perpendicular to a *single* thin ferromagnetic layer can excite spin waves in the ferromagnet.²⁸ These spin waves have wavevector perpendicular to the direction of current flow. The key mechanism behind the transverse spin wave instability is electron diffusion in the normal-metal contacts perpendicular to the direction of current flow, see Fig. 1. Electrons backscattered from the ferromagnet are spin polarized, the polarization direction being antiparallel to the direction of the magnetization at the location where they were reflected from the ferromagnet. When these electrons reach the ferromagnetic layer a second time, they typically do so at a different point at the normal-metal–ferromagnet interface. In the presence of a spin wave, the magnetization direction of the ferromagnet will be different at that point, and these electrons will transfer the perpendicular component of their spin to the ferromagnet, thus exerting a spin-transfer torque. The sign of this torque is to enhance the spin-wave amplitude. A similar argument can be made for electrons transmitted through the ferromagnet, but their torques tend to suppress the spin-wave amplitude. Typically, source and drain contacts are asymmetric, and a net spin-transfer torque is exerted on the ferromagnet. This torque leads

*Present address: Département de Physique Théorique, Université de Genève, CH-1211 Genève 4, Switzerland

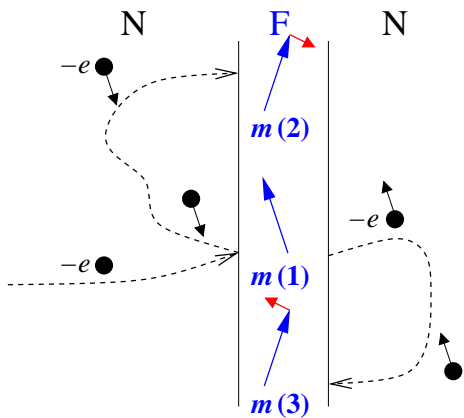


FIG. 1: Through the spin-transfer torque, an unpolarized electrical current flowing perpendicular to a thin ferromagnetic layer can enhance or suppress spin waves. Electrons *backscattered* from the ferromagnet at point 1 have their spin predominantly polarized antiparallel to magnetization direction $\mathbf{m}(1)$. These electrons exert a torque on the ferromagnet's magnetization $\mathbf{m}(2)$ if they reach the ferromagnet a second time at point 2, the direction of the torque being to enhance an existing spinwave [*i.e.*, to increase any pre-existing difference between $\mathbf{m}(1)$ and $\mathbf{m}(2)$]. When electrons *transmitted* through the ferromagnet reach the ferromagnet a second time at point 3, they exert a torque that suppresses an existing spinwave. If source and drain contacts are not symmetric, there is a net torque on the ferromagnet, which enhances or suppresses the spin wave, depending on current direction.

to a spin wave instability for the current direction in which the effect of backscattered electrons dominates, and not for the other current direction. Experiments on nanopyllars with a single ferromagnetic layer have verified the theoretical predictions finding spin-wave instabilities for one direction of the current and for asymmetric junctions only.²⁹

For a quantitative theory of this transverse spin-wave instability, an approach that combines a full self-consistent determination of the spin-transfer torque and, at the same time, goes beyond the macrospin approximation is essential.²⁸ Indeed, the macrospin approximation does not allow for non-uniform spin waves in the ferromagnet, and, whereas an externally imposed spin transfer torque would predict a similar instability, a non-self-consistent theory would be quantitatively incorrect (*e.g.* predict the wrong wavelength for the spin wave) because it neglects the coupling between the spin current and the spin waves in the ferromagnet.

The possibility of current-induced non-uniform modes in heterostructures has become of recent interest in the field, both for single-layer and multilayer structures.^{30,31,32,33,34,35} In particular, Ji, Chien, and Stiles³⁰ reported experimental and theoretical evidence that for large ferromagnet thickness, ferromagnet-normal-metal junctions are unstable to the generation of non-uniform magnetization modes, but in this case, these are longitudinal modes (see also Refs. 6 and 36). Further,

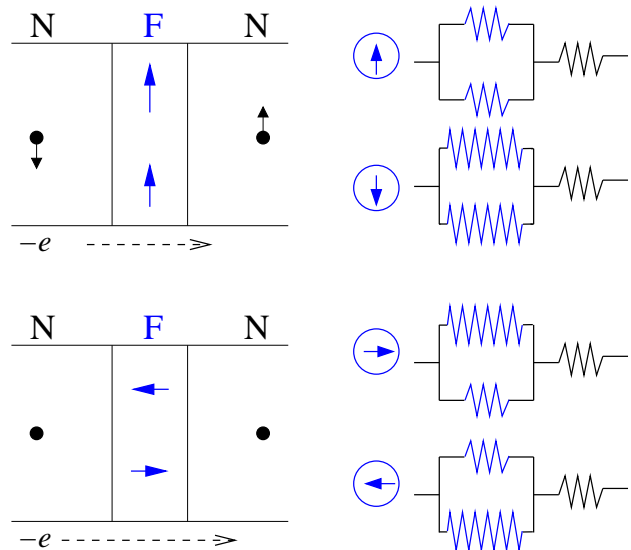


FIG. 2: Spin will accumulate in normal metals on both sides of a ferromagnetic layer with uniform magnetization if an unpolarized current is passed through the ferromagnet (top left). A large-amplitude spinwave in the ferromagnet reduces the amount of spin polarization in the normal-metal regions adjacent to the ferromagnet and lowers the total resistance of the device (bottom left). This is shown schematically in the circuit diagrams (right). The top two circuit diagrams show the resistances seen by majority and minority electrons when the magnetization is spatially uniform, the short and long resistor symbols referring to minority and majority resistances, respectively. The ferromagnet with a large-amplitude spin wave can be seen as a parallel configuration of ferromagnets with opposite magnetization directions. The bottom two circuit diagrams show the resistances seen by two spin directions in this case. The net resistance is lower in the presence of a large-amplitude spin wave.

Stiles, Xiao, and Zangwill pointed out that transverse spinwaves can be excited even in symmetric junctions if the spinwave mode is at not uniform in the direction of current flow. However, excitation of these modes requires a higher currents than the transverse spin-waves considered here.³¹

Our previous work,²⁸ as well as the other theoretical works on this and related spin-wave instabilities,^{31,34} was a linear stability analysis, sufficient to predict the onset of the instability, but not to describe the spin wave amplitude for current densities larger than the critical current density. Knowledge of the spin wave amplitude is necessary if one wants to study, *e.g.*, how the spin wave instability affects the resistance of the normal-metal-ferromagnet junction. It is the goal of this present work to examine in detail the dynamics of the spin-wave beyond the instability. While we focus on the case of single-layers, we expect that, in light of the work of Refs. 32,34, our qualitative findings will carry over to the case of trilayers and heterojunctions.

Although a quantitative description of how the spin-wave instability affects the resistance of the normal-

metal–ferromagnet junction will be postponed to the next two sections, the sign of the effect can be determined using simple considerations. Once the current density has exceeded the critical current density for the spin wave excitation and a spin wave has been established, the fact that the magnetization is no longer uniform reduces the amount of spin accumulation in the normal metal contacts adjacent to the ferromagnet. A reduction of the spin accumulation in the normal metal contacts causes a reduction of the sample’s resistance, see Fig. 2 for a schematic drawing. Indeed, the experiments of Ref. 29 observed a small decrease of the resistance of the nanopillar upon onset of the spin-wave instability. The effect of a purely transverse spinwave instability is opposite to that of a longitudinal spinwave, which increases the resistance of the device.³⁶ The reduction of the spin accumulation in the normal-metal spacer also lowers the spin-transfer torque, thus providing a mechanism to saturate the growth of the spin wave amplitude for current densities larger than the critical current density. Moreover, note that a theory of this effect needs to combine features of both the micromagnetic approach and the self-consistent treatment of the spin-transfer torque.

In Sec. II we consider current densities slightly above the critical current density. In this regime, a perturbative treatment in the spin wave amplitude is possible. In Sec. III we then perform a detailed numerical simulation of a simplified system that allows us to probe current densities much larger than the critical current density. Whereas the observed magnetization dynamics in the presence of a large magnetic field is rather unsurprising — there is one stable energy minimum, and the magnetization precesses around the direction for which energy is minimal —, in the absence of an external magnetic field we find a hierarchy of instabilities. For very high currents the system shows chaotic behavior with measurable Lyapunov exponents.

II. PERTURBATIVE CALCULATION

We consider a single ferromagnetic layer, connected to source and drain reservoirs, see Fig. 3. Between the ferromagnet and the drain reservoir is a normal-metal spacer, as is common in nanopillar geometries. There is, however, no normal-metal spacer between the ferromagnet and the source reservoir. We use coordinates x , y , z , where x is the coordinate perpendicular to the layer structure and y and z are coordinates in the plane of the layers.

Both the ferromagnet and the spacer layer have a rectangular cross section of dimensions $W_y \times W_z$. The ferromagnet has thickness d , which is taken small enough that the chemical potential for the conduction electrons and the direction \mathbf{m} of the magnetization of the ferromagnet do not depend on the longitudinal coordinate x . The normal metal spacer has thickness L . Transport through the normal metal spacer is diffusive, with conductivity σ .

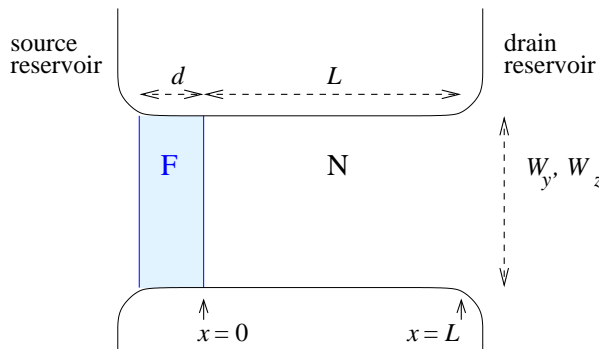


FIG. 3: Schematic picture of the normal-metal–ferromagnet–normal-metal junction considered in our calculations. The ferromagnetic layer (F) is connected to source and drain reservoirs through normal metal spacers (N). We consider the maximally asymmetric case with only one spacer of length $L \gg l_{sf}$.

In the normal metal spacer, the charge and spin degrees of the conduction electrons are described by the equations

$$\begin{aligned} \nabla^2 \mu_c &= 0, & j_x &= (\sigma/e) \partial_x \mu_c, \\ l_{sf}^2 \nabla^2 \boldsymbol{\mu}_s &= \boldsymbol{\mu}_s, & \mathbf{j}_s &= -(\hbar\sigma/2e^2) \partial_x \boldsymbol{\mu}_s, \end{aligned} \quad (1)$$

where μ_c and $\boldsymbol{\mu}_s$ are chemical potentials for the electron density and electron spin respectively, $-e$ is the electron charge, and l_{sf} is the spin diffusion length in the normal metal spacer. Further, j_x is the charge current density and σ is the conductivity of the normal metal leads. The boundary conditions for $x = L$ at the drain reservoir is

$$\mu_c(L) = -eV, \quad \boldsymbol{\mu}_s(L) = \mathbf{0}. \quad (2)$$

Here the argument L refers to the x coordinate. The y and z coordinates are not written explicitly. The second boundary is the interface between the normal-metal and ferromagnet at $x = 0$. Since the electron dynamics happens on a time scale that is much faster than the rate of change of the magnetization direction \mathbf{m} , this boundary condition can be taken treating \mathbf{m} in the adiabatic approximation,^{26,27}

$$\begin{aligned} j_x(0) &= \frac{1}{e} [g_+ \mu_c(0) + g_- \mathbf{m} \cdot \boldsymbol{\mu}_s(0)], \\ \mathbf{j}_s(0) &= -\frac{\hbar}{2e^2} (g_- \mu_c(0) + g_+ \mathbf{m} \cdot \boldsymbol{\mu}_s(0)) \mathbf{m} \\ &\quad + \frac{\hbar}{2e^2} g_1 (2\boldsymbol{\mu}_s(0) \times \mathbf{m} + \hbar \dot{\mathbf{m}}) \times \mathbf{m} \\ &\quad + \frac{\hbar}{2e^2} g_2 (2\boldsymbol{\mu}_s(0) \times \mathbf{m} + \hbar \dot{\mathbf{m}}). \end{aligned} \quad (3)$$

Here $g_{\pm} = (g_{\uparrow} \pm g_{\downarrow})/2$, where g_{\uparrow} and g_{\downarrow} are interface conductivities for spins aligned parallel and anti-parallel to \mathbf{m} , and $g_1 + ig_2$ is the complex valued ‘mixing interface conductivity’. The argument ‘0’ refers to a coordinate in the normal metal spacer, just outside the ferromagnetic layer. The charge current and the spin current parallel

to \mathbf{m} are continuous at the interface. In writing down Eq. (3) we assumed that the two ferromagnet–normal-metal interfaces are identical, so that the potentials μ_c and $\mathbf{m} \cdot \boldsymbol{\mu}_s$ drop equally over both interfaces of the ferromagnet; the component of $\boldsymbol{\mu}_s$ perpendicular to \mathbf{m} is zero in the ferromagnet. (It is the non-conservation of spin current perpendicular to \mathbf{m} that gives rise to the spin transfer torque.) For Co/Cu and Fe/Cr interfaces, these conductivities are tabulated, see Refs. 14,37. Typical values are in the range $g_2 \ll g_1 \sim g_{\pm} \sim 10^{14} \Omega^{-1} m^{-2}$. For any interface, one has the constraint $g_1 > g_+ > g_-$.²⁶

We are interested in the situation in which the magnetization is allowed to vary in the direction perpendicular to the current flow. In this case a large enough current may cause spin-wave excitations perpendicular to the direction of current flow.²⁸ To simplify the notation, we take the limit $L \gg l_{sf}$. The spin and charge chemical potentials in the normal-metal spacer then have the general solution

$$\begin{aligned} \mu_c(\mathbf{r}) &= \sum_{\mathbf{q}} e^{iq_y y + iq_z z} a_c(\mathbf{q}) e^{-(q_y^2 + q_z^2)^{1/2} x} + \frac{eIx}{W_y W_z \sigma}, \\ \mu_s(\mathbf{r}) &= \sum_{\mathbf{q}} e^{iq_y y + iq_z z} e^{-(q_y^2 + q_z^2 + l_{sf}^{-2})^{1/2} x} \mathbf{a}_s(\mathbf{q}), \end{aligned} \quad (4)$$

where $\mathbf{q} = (0, q_y, q_z)^T$ is a wavevector in the y - z plane. The components q_y and q_z take values $q_y = \pi n_y / W_y$, $q_z = \pi n_z / W_z$ with integers n_y and n_z . The Fourier expansion coefficients $a_c(\mathbf{q})$ and $\mathbf{a}_s(\mathbf{q})$ are real and satisfy

$$a_c(\mathbf{q}) = a_c(-\mathbf{q}), \quad \mathbf{a}_s(\mathbf{q}) = \mathbf{a}_s(-\mathbf{q}). \quad (5)$$

We further define the quantities

$$\begin{aligned} G_c(\mathbf{q}) &= (\sigma/2)(q_y^2 + q_z^2)^{1/2}, \\ G_s(\mathbf{q}) &= (\sigma/2)(q_y^2 + q_z^2 + l_{sf}^{-2})^{1/2}, \end{aligned} \quad (6)$$

which have the same dimension as the interface conductivities g_{\pm} , g_1 , and g_2 . With these definitions, the boundary condition (3) at the normal-metal–ferromagnet interface becomes

$$\begin{aligned} 0 &= -\frac{eI}{W_y W_z} + 2 \sum_{\mathbf{q}} e^{iq_y y + iq_z z} [G_c(\mathbf{q}) a_c(\mathbf{q}) + g_+ a_c(\mathbf{q}) + g_- \mathbf{a}_s(\mathbf{q}) \cdot \mathbf{m}], \\ 0 &= \sum_{\mathbf{q}} e^{iq_y y + iq_z z} [2G_s(\mathbf{q}) \mathbf{a}_s(\mathbf{q}) + (g_- a_c(\mathbf{q}) \mathbf{m} + g_+ \mathbf{a}_s(\mathbf{q}) \cdot \mathbf{m}) \mathbf{m} - 2g_1 (\mathbf{a}_s(\mathbf{q}) \times \mathbf{m}) \times \mathbf{m} - 2g_2 \mathbf{a}_s(\mathbf{q}) \times \mathbf{m}] \\ &\quad - \hbar g_1 \dot{\mathbf{m}} \times \mathbf{m} - \hbar g_2 \dot{\mathbf{m}}. \end{aligned} \quad (8)$$

Although Eq. (8) gives a set of linear equations for the expansion coefficients $a_c(\mathbf{q})$ and $\mathbf{a}_s(\mathbf{q})$, a solution in closed form is not possible for arbitrary magnetization $\mathbf{m}(y, z)$. Instead, we expand around the uniform equilibrium direction. Hereto we introduce a second coordinate system with axes labeled 1, 2, and 3, such that \mathbf{m} points along the unit vector \mathbf{e}_3 in the absence of an applied current, and write

$$\mathbf{m} = m_1 \mathbf{e}_1 + m_2 \mathbf{e}_2 + (1 - m_1^2 - m_2^2)^{1/2} \mathbf{e}_3. \quad (9)$$

We then perform a Fourier transform, similar to Eq. (4)

$$m_j(y, z) = \sum_{\mathbf{q}} m_j(\mathbf{q}) e^{iq_y y + iq_z z}, \quad j = 1, 2, \quad (10)$$

where $m_j(\mathbf{q}) = m_j(-\mathbf{q})$. Finally, expanding in powers of m_1 and m_2 , we have solved the spin and charge chemical potentials to third order in m_1 and m_2 , which parameterize the deviations from equilibrium.

In order to complete the calculation, we need to calculate the rate of change of the magnetization direction

\mathbf{m} in the presence of the current I . Hereto we use the Landau-Lifshitz-Gilbert equation,^{38,39}

$$\dot{\mathbf{m}} = \alpha \mathbf{m} \times \dot{\mathbf{m}} + \boldsymbol{\tau}_{ex} + \boldsymbol{\tau}_{an} + \boldsymbol{\tau}_{ne}, \quad (11)$$

where α is the Gilbert damping coefficient, $\boldsymbol{\tau}_{ex}$ is the torque arising from exchange, $\boldsymbol{\tau}_{an}$ is the torque from the combined effect of magnetic anisotropy and an applied magnetic field, and $\boldsymbol{\tau}_{ne}$ represents the current-induced spin-transfer torque. The latter reads⁴⁰

$$\begin{aligned} \boldsymbol{\tau}_{ne} &= \frac{\gamma}{Md} (\mathbf{j}_s(0) - \mathbf{j}_s(-d)) \times \mathbf{m} \times \mathbf{m} \\ &= -\frac{\hbar\gamma}{Mde^2} [g_1 (\boldsymbol{\mu}_s \times \mathbf{m} + \hbar \dot{\mathbf{m}}) \times \mathbf{m} \\ &\quad + g_2 (\boldsymbol{\mu}_s \times \mathbf{m} + \hbar \dot{\mathbf{m}})]. \end{aligned} \quad (12)$$

Here the spin current $\mathbf{j}_s(-d)$ is taken in the source reservoir, M is the magnetization per unit volume and γ is the gyromagnetic ratio. Note that the terms proportional to the time derivative $\dot{\mathbf{m}}$ have contributions from two interfaces while the contribution to the torque from the spin

chemical potential has a contribution from the $x = 0$ interface only. (All potentials are zero in the source reservoir.) The exchange torque $\boldsymbol{\tau}_{\text{ex}}$ is

$$\boldsymbol{\tau}_{\text{ex}} = J\gamma M\nabla^2\mathbf{m} \times \mathbf{m}, \quad (13)$$

where J is the exchange constant. To linear order in m_1 and m_2 , the anisotropy torque $\boldsymbol{\tau}_{\text{an}}$ can be written

$$\boldsymbol{\tau}_{\text{an}} = -\frac{\gamma}{M}(k_1m_1\mathbf{e}_1 + k_2m_2\mathbf{e}_2) \times \mathbf{m}, \quad (14)$$

where k_1 and k_2 describe the combined effect of magnetic anisotropy and an applied magnetic field. If anisotropy dominates over the effect of a magnetic field, higher-order terms in an expansion in powers of m_1 and m_2 will be highly sample specific. Although this case can be dealt with using the methods presented below, the result of the calculation has little predictive value if those coefficients are not known independently. Therefore, we focus on the opposite limit that the anisotropy term in Eq. (14) is dominated by magnetic field. Then higher-order terms in an expansion in powers of m_1 and m_2 are related to the first-order terms, and one has

$$\boldsymbol{\tau}_{\text{an}} = (k\gamma/M)\mathbf{e}_3 \times \mathbf{m}. \quad (15)$$

where we wrote $k_1 = k_2 = k$. For future reference, we combine the material constants J and $2k = k_1 + k_2$ into the combinations

$$q_{\text{f}}^2 = \frac{k}{JM^2}, \quad j_{\text{f}}^2 = \left(\frac{2e}{\hbar}\right)^2 JM^2k, \quad (16)$$

which have the dimension of inverse length and current density, respectively.

We now proceed to report the result of our calculation. The lowest order result, indicated by a superscript “(0)”, is

$$\begin{aligned} a_{\text{c}}^{(0)}(\mathbf{q}) &= \frac{ej(g_+ + 2G_{\text{s}}(0))}{g_{\text{m}}(0)g_-} \delta_{\mathbf{q},0}, \\ \mathbf{a}_{\text{s}}^{(0)}(\mathbf{q}) &= \frac{-ej}{g_{\text{m}}(0)} \mathbf{e}_3 \delta_{\mathbf{q},0}. \end{aligned} \quad (17)$$

Here $j = I/W_yW_z$ is the current density and²⁸

$$g_{\text{m}}(\mathbf{q}) = \frac{(g_+ + 2G_{\text{s}}(\mathbf{q}))(g_+ + 2G_{\text{c}}(\mathbf{q}))}{g_-} - g_-. \quad (18)$$

Writing $\mu_{\text{c}}(L) = -eV = -e(L/\sigma W_yW_z + R)I$, we conclude that the resistance R of the ferromagnetic layer is

$$R = \frac{2}{W_yW_z} \frac{\sigma/l_{\text{sf}} + g_+}{2g_+\sigma/l_{\text{sf}} + g_+^2 - g_-^2}. \quad (19)$$

For the zeroth-order solution, the spin potential μ_{s} is collinear with \mathbf{m} throughout the sample. Hence, to that order there is no current-induced torque. This is different when small deviations from the situation $\mathbf{m} = \mathbf{e}_3$ are taken into account to first order. One finds that the first-order corrections $a_{\text{c}}^{(1)}(\mathbf{q})$ and $a_{\text{s}3}^{(1)}(\mathbf{q})$ are zero. In order to represent the first-order contributions to the transverse spin potentials $a_{\text{s}1}$ and $a_{\text{s}2}$, we use spinor notation, $a_{\text{s}} = (a_{\text{s}1}, a_{\text{s}2})^{\text{T}}$ and $m = (m_1, m_2)^{\text{T}}$. Then, defining

$$D(\mathbf{q}) = (g_1 + G_{\text{s}}(\mathbf{q}))^2 + g_2^2, \quad (20)$$

we find

$$\begin{aligned} a_{\text{s}}^{(1)}(\mathbf{q}) &= -\frac{ej}{g_{\text{m}}(0)}m(\mathbf{q}) + \frac{ej(G_{\text{s}}(\mathbf{q}) - G_{\text{s}}(0))}{g_{\text{m}}(0)D(\mathbf{q})} [(g_1 + G_{\text{s}}(\mathbf{q}))m(\mathbf{q}) + ig_2\sigma_2m(\mathbf{q})] \\ &\quad + \frac{\hbar}{2D(\mathbf{q})} [g_2G_{\text{s}}(\mathbf{q})\dot{m}(\mathbf{q}) + (g_1^2 + g_1G_{\text{s}}(\mathbf{q}) + g_2^2)i\sigma_2\dot{m}(\mathbf{q})]. \end{aligned} \quad (21)$$

where σ_2 is the second Pauli matrix. Note that the first term on the right hand side is the response to a uniform rotation of the magnetization, while the second and third terms give the response to a non-uniform and time-dependent magnetization.

The potentials are substituted into Eq. (12) to find the current-induced torque, and then into the Landau-Lifshitz-Gilbert equation (11) to find the rate of change of the magnetization. The current-induced torque has contributions proportional to the time derivative $\dot{\mathbf{m}}$, which lead to a renormalization of the Gilbert damping param-

eter α and the gyromagnetic ratio γ . The renormalized Gilbert damping parameter $\tilde{\alpha}$ and gyromagnetic ratio $\tilde{\gamma} = \gamma/\tilde{\beta}$ depend on the transverse wavevector \mathbf{q} and read

$$\begin{aligned} \tilde{\alpha} &= \alpha + \frac{\hbar^2\gamma(g_1 + G_{\text{s}}(\mathbf{q}))}{2Mde^2} \left[1 - \frac{G_{\text{s}}(\mathbf{q})^2}{D(\mathbf{q})}\right], \\ \tilde{\beta} &= 1 + \frac{\hbar^2\gamma g_2}{2Mde^2} \left[1 + \frac{G_{\text{s}}(\mathbf{q})^2}{D(\mathbf{q})}\right]. \end{aligned} \quad (22)$$

In the macrospin limit $q \rightarrow 0$, these modifications coincide with the renormalized values originally reported in

Ref. 27.

Again using two-component spinor notation, the complete Landau-Lifshitz-Gilbert equation then becomes

$$(\tilde{\beta}\mathbb{1}_2 + i\sigma_2\tilde{\alpha})\dot{m}(\mathbf{q}) = A(\mathbf{q})m(\mathbf{q}), \quad (23)$$

with

$$A(\mathbf{q}) = \tau_{\parallel}^{(1)}\mathbb{1}_2 - i\sigma_2 \left[\tau_{\perp}^{(1)} + \frac{\hbar\gamma j_{\text{f}}(q^2 + q_{\text{f}}^2)}{2eq_{\text{f}}M} \right] + \sigma_3 \frac{\gamma(k_1 - k_2)}{2M} \quad (24)$$

and

$$\begin{aligned} \tau_{\parallel}^{(1)}(\mathbf{q}) &= \frac{\hbar\gamma e j}{Mde^2} \frac{g_1^2 + g_2^2 + g_1 G_{\text{s}}(\mathbf{q})}{g_{\text{m}}(0)D(\mathbf{q})} [G_{\text{s}}(\mathbf{q}) - G_{\text{s}}(0)], \\ \tau_{\perp}^{(1)}(\mathbf{q}) &= \frac{\hbar\gamma e j}{Mde^2} \frac{g_2 G_{\text{s}}(\mathbf{q})}{g_{\text{m}}(0)D(\mathbf{q})} [G_{\text{s}}(\mathbf{q}) - G_{\text{s}}(0)]. \end{aligned} \quad (25)$$

In the absence of a current, any spatial modulation of the magnetization is damped. However, a sufficiently large positive current I can overcome the damping, and cause a spatial modulation of \mathbf{m} to grow in time, rather than decay. (A positive current I corresponds to electron flow in the negative x direction.) The instability condition is easily obtained from Eq. (23)

$$\tau_{\parallel}^{(1)}(\mathbf{q}) \frac{\tilde{\beta}(\mathbf{q})}{\tilde{\alpha}(\mathbf{q})} > \frac{\hbar\gamma j_{\text{f}}(q^2 + q_{\text{f}}^2)}{2eq_{\text{f}}M} + \tau_{\perp}^{(1)}(\mathbf{q}). \quad (26)$$

We can analyze this result in different limits. For a ferromagnetic layer with sufficiently small transverse dimensions, $W_y, W_z \lesssim (l_{\text{sf}}/q_{\text{f}}^2)^{1/3}$ if $l_{\text{sf}}q_{\text{f}} \gg 1$, the instability happens at wavevector $\mathbf{q} = (\pi/W_y)\hat{y}$ or $\mathbf{q} = (\pi/W_z)\hat{z}$, whichever is smallest, and the critical current follows directly from Eq. (26). For wider layers, the critical current density j_c and critical wavevector \mathbf{q}_c are found as the current-density wavevector pair for which the onset of the instability condition happens at the lowest current density.

This condition can be simplified in the limit of a very thin ferromagnetic layer, $d \rightarrow 0$, neglecting terms proportional to g_2 (which is numerically smaller than g_1), and for wavenumbers $q \ll q_{\text{f}}$. We then find that the critical current follows from minimizing the relation

$$j_c(\mathbf{q}) = \frac{\hbar^2\gamma g_{\text{m}}(0)j_{\text{f}}}{2Mq_{\text{f}}e^2} \frac{q^2 + q_{\text{f}}^2}{1 - (1 + q^2l_{\text{sf}}^2)^{-1/2}}. \quad (27)$$

In the limit $l_{\text{sf}} \gg 1/q_{\text{f}}$, this gives²⁸

$$q_c = (q_{\text{f}}^2/2l_{\text{sf}})^{1/3}, \quad j_c = \frac{\hbar^2\gamma g_{\text{m}}(0)q_{\text{f}}j_{\text{f}}}{2Me^2}. \quad (28)$$

(The result for j_c was reported incorrectly in Ref. 28. Note that the condition $q_c \ll q_{\text{f}}$, which was used to derive Eq. (27) is consistent with Eq. (28) if $l_{\text{sf}} \gg 1/q_{\text{f}}$.) Note that q_{f} increases with an applied magnetic field, so that this limit becomes relevant even for the case of a normal

metal with strong spin relaxation if the magnetic field is large enough. In the limit $l_{\text{sf}} \ll 1/q_{\text{f}}$ of strong spin relaxation and weak anisotropy, one has

$$q_c = (4/3)^{1/4}(q_{\text{f}}/l_{\text{sf}})^{1/2}, \quad j_c = \frac{\hbar^2\gamma g_{\text{m}}(0)j_{\text{f}}}{Mq_{\text{f}}l_{\text{sf}}^2e^2}. \quad (29)$$

At the critical current density, the trajectory of the magnetization is a simple ellipse (circle in the case of large magnetic fields). The ellipse is described by the coordinate transformation $m_1 = r(\cos\theta \cos\phi + \eta \sin\theta \sin\phi)$, and $m_2 = r(\sin\theta \cos\phi - \eta \cos\theta \sin\phi)$. The solution of the magnetization dynamics at the critical current then gives $\phi = \omega_0 t$ and r constant, where $\omega_0^2 = \omega_+^2 - \omega_-^2$, $\eta = (\omega_+ - \omega_-)/\omega_0$ and

$$\omega_+^{-1} = \frac{2Mce^2q_{\text{f}} \cos(2\theta)}{\gamma(q_{\text{f}}^2 + q_c^2)j_{\text{f}}} - \frac{2Mce^2q_{\text{f}}g_2G_{\text{s}}(\mathbf{q}) \sin(2\theta)}{\gamma j_{\text{f}}(q_{\text{f}}^2 + q_c^2)(g_1^2 + g_2^2 + g_1G_{\text{s}}(\mathbf{q}))}, \quad (30)$$

$$\omega_-^{-1} = \frac{2Mc\hbar}{\gamma(k_1 - k_2)}. \quad (31)$$

and c, θ are obtained from $\tilde{\alpha} = c \sin 2\theta, \tilde{\beta} = c \cos 2\theta$. For the case of a large applied magnetic field, $k_1 = k_2 = k$, and neglecting g_2 , we have $\eta = 1$ and

$$\omega_0 = \hbar\gamma j_{\text{f}}(q_c^2 + q_{\text{f}}^2)/(2eq_{\text{f}}M). \quad (32)$$

Note that, although the applied current has a large effect on the stability of the ellipsoidal motion (precession is damped for $j < j_c$ and unstable for $j > j_c$), its effect on the precession frequency is small. To a good approximation, the precession frequency equals the ferromagnetic resonance frequency in the absence of a current.

Whereas the first-order calculation allows one to find the current density at which the spin-wave instability sets in and the angular form of the low-amplitude excitations, it does not provide information about the magnitude of the spinwave oscillation for $j > j_c$, or about the effect of the spinwave oscillation on the resistance of the ferromagnetic layer. This information can only be obtained from the analysis of the magnetization dynamics beyond first-order in the amplitude. Such a program proceeds along the same lines as the first-order calculation shown above: Calculation of the potentials for charge and spin in the presence of a non-uniform and time-dependent magnetization, followed by a calculation of the current-induced torque and the rate of change of the magnetization. We have carried out this program to third order in m_1 and m_2 , and list some of our general results in the appendix. However, as this calculation involves higher-order contributions to the anisotropy torque $\boldsymbol{\tau}_{\text{an}}$, for which the expansion constants are unknown, we find that this calculation has little predictive value. Instead, we focus on the limit in which all magnetic anisotropy arises from an applied magnetic field. In this limit, $\boldsymbol{\tau}_{\text{an}}$ is known, cf. Eq. (15), and a theoretical analysis is useful.

An important simplification is that the higher-order analysis is necessary for the Fourier components $m_1(\mathbf{q}_c)$ and $m_2(\mathbf{q}_c)$ at the critical wavevector only. Hence, we need to consider only a single Fourier component in our considerations below. Solving for the leading (second order) correction to the charge potential, we find an expression that depends on the magnetization amplitude, to second order in m_1 and m_2 , and on the time derivatives. Only first-order time-derivatives appear, which can be eliminated using the Landau-Lifshitz-Gilbert equation (23). For the case of a large applied magnetic field, the magnetization precession is circular, and one has

$$m_1(\mathbf{q}_c)\dot{m}_2(\mathbf{q}_c) - m_2(\mathbf{q}_c)\dot{m}_1(\mathbf{q}_c) = \omega_0 r(\mathbf{q}_c)^2, \quad (33)$$

where we abbreviated

$$r(\mathbf{q}_c)^2 = m_1(\mathbf{q}_c)^2 + m_2(\mathbf{q}_c)^2. \quad (34)$$

The precession frequency ω_0 given by Eq. (30) above. We then find

$$\begin{aligned} a_c^{(2)}(0) &= \frac{2(G_s(0) - G_s(\mathbf{q}_c))r(\mathbf{q}_c)^2}{D(\mathbf{q}_c)g_m(0)^2} \\ &\times [\omega_0 g_m(0) (D(\mathbf{q}_c) - G_s(\mathbf{q}_c)(g_1 + G_s(\mathbf{q}_c))) \\ &- 2ej_c (D(\mathbf{q}_c) + (G_s(0) - G_s(\mathbf{q}_c))(g_1 + G_s(\mathbf{q}_c)))] \end{aligned} \quad (35)$$

Solving for the leading (third) order torque, we note that the third order torque depends not only on the mag-

netization amplitudes $m_1(\mathbf{q}_c)$ and $m_2(\mathbf{q}_c)$, but also on their time derivative \dot{m}_1 and \dot{m}_2 . The time derivatives appear to first, second, and third order in the expansion. The dependence on $\dot{m}^{(3)}$ leads to the same modifications to the Gilbert damping and gyromagnetic ratio as for the first-order current-induced torque calculated above. The dependence on $\dot{m}^{(2)}$ is through the 3-component only, which can be written as

$$\dot{m}_3^{(2)} = -m_1\dot{m}_1^{(1)} - m_2\dot{m}_2^{(1)}. \quad (36)$$

The first-order time derivatives $\dot{m}^{(1)}$ can be expressed in terms of m_1 and m_2 using Eq. (33) [or, in the general case, using Eq. (23)]. For the anisotropy torque τ_{an} we take the contribution from the magnetic field only. Hence,

$$\begin{aligned} \tau_{\text{ex}}(\mathbf{q}_c) + \tau_{\text{an}}(\mathbf{q}_c) &= \frac{\hbar\gamma j_{\text{f}}}{2eq_{\text{f}}M} \left[q_c^2 + q_{\text{f}}^2 + \frac{q_c^2}{2} r(\mathbf{q}_c)^2 \right] \\ &\times (-i\sigma_2)m(\mathbf{q}_c). \end{aligned} \quad (37)$$

Thus proceeding, we find that the third-order equation for the rate of change of the magnetization direction reads

$$(\tilde{\beta}\mathbb{1}_2 + i\sigma_2\tilde{\alpha})\dot{m}(\mathbf{q})^{(3)} = A(\mathbf{q})^{(3)}m(\mathbf{q})^{(3)}, \quad (38)$$

with

$$A(\mathbf{q}_c)^{(3)} = -\frac{1}{2}r(\mathbf{q}_c)^2 \left[2\tau_{\parallel}^{(3)}(0)\mathbb{1}_2 - 2i\sigma_2\tau_{\perp}^{(3)}(0) + \tau_{\parallel}^{(3)}(2\mathbf{q}_c)\mathbb{1}_2 - i\sigma_2\tau_{\perp}^{(3)}(2\mathbf{q}_c) + 3\tilde{\alpha}\omega_0\mathbb{1}_2 + \frac{\hbar\gamma j_{\text{f}}q_c^2}{2eq_{\text{f}}M}i\sigma_2 \right], \quad (39)$$

and

$$\begin{aligned} \tau_{\parallel}^{(3)}(\mathbf{k}) &= \frac{\hbar\gamma g_1}{Mde^2(g_1 + G_{\mathbf{q}})} \left\{ \frac{[g_+ + 2G_c(\mathbf{k})][g_+ + 2G_s(\mathbf{q})] - g_-^2}{[g_+ + 2G_c(\mathbf{k})][g_+ + 2G_s(\mathbf{k})] - g_-^2} \right\} \\ &\times \left\{ \frac{ej}{g_m(0)}[G_s(\mathbf{k}) - G_s(0)] + \left[g_1\hbar\omega_0 - \frac{2ej(g_1 + G_s(0))}{g_m(0)} \right] \frac{G_s(\mathbf{k}) - G_s(\mathbf{q})}{g_1 + G_s(\mathbf{q})} \right\}, \end{aligned} \quad (40a)$$

$$\begin{aligned} \tau_{\perp}^{(3)}(\mathbf{k}) &= \frac{\hbar\gamma g_2 G_s(\mathbf{q})[G_s(\mathbf{k}) - G_s(\mathbf{q})]}{Mde^2[g_1 + G_s(\mathbf{q})]^3} \left\{ \frac{[g_+ + 2G_c(\mathbf{k})][g_+ + 2G_s(\mathbf{q})] - g_-^2}{[g_+ + 2G_c(\mathbf{k})][g_+ + 2G_s(\mathbf{k})] - g_-^2} \left[g_1\hbar\omega_0 - \frac{ej(g_1 + G_s(0))}{g_m(0)} \right] \right. \\ &\left. + \frac{[(g_+ - 2g_1)(2G_c(\mathbf{k}) + g_+) - g_-^2][G_s(\mathbf{q}) - G_s(0)]ej}{g_m(0)[(g_+ + 2G_c(\mathbf{k}))(g_+ + 2G_s(\mathbf{k})) - g_-^2]} \right\}. \end{aligned} \quad (40b)$$

Solving the differential equation for m , one finds that the precession amplitude for current density j slightly above the critical current density j_c reads

$$r(\mathbf{q}_c)^2 = \frac{\hbar\gamma j_{\text{f}}(j - j_c)}{eq_{\text{f}}Mj_c} \frac{\tilde{\alpha}(q_c^2 + q_{\text{f}}^2)}{\tilde{\beta} \left[2\tau_{\parallel}^{(3)}(0) + \tau_{\parallel}^{(3)}(2\mathbf{q}_c) - 3\tau_{\parallel}^{(1)}(\mathbf{q}_c) \right] - \tilde{\alpha} \left[2\tau_{\perp}^{(3)}(0) + \tau_{\perp}^{(3)}(2\mathbf{q}_c) - \hbar\gamma j_{\text{f}}q_c^2/(2eq_{\text{f}}M) \right]}. \quad (41)$$

The result takes a simpler form in the limit $g_2 \rightarrow 0$ (since g_2 is numerically smaller than g_1), $d \rightarrow 0$, and $1/l_{\text{sf}} \ll$

$q_c \ll q_f$,

$$r(\mathbf{q}_c)^2 = \frac{(j - j_c)(g_+^2 - g_-^2 + g_+\sigma/l_{sf})}{j_c(2g_1g_+ + g_+\sigma/l_{sf} - g_+^2 + g_-^2)}. \quad (42)$$

Since $g_1 > g_+ > g_-$ we conclude that the $r(\mathbf{q}_c)^2 > 0$ is positive if $j > j_c$, which excludes hysteretic behavior.

In the same limit we can also calculate the change in frequency of the spinwave given by

$$\frac{\omega}{\omega_0} = 1 + \frac{q_c^2 r(\mathbf{q}_c)^2}{3(q_c^2 + q_f^2)}. \quad (43)$$

Since the prefactor of the second term is much smaller than unity, $q_c \ll q_f$ for the parameter regime of interest, we conclude that in the regime of perturbation theory, there is hardly any change from the ferromagnetic resonance frequency.

Finally, at the onset of the spin-wave instability, the resistance of the ferromagnetic layer acquires a small negative correction

$$\begin{aligned} \frac{R}{R_0} &= 1 + \frac{a_c^{(2)}(0)}{a_c^{(0)}(0)}, \\ &\approx 1 - \frac{2(\sigma/l_{sf} + 3g_1)g_-^2 r(\mathbf{q}_c)^2}{(\sigma/l_{sf} + g_+)(g_+^2 - g_-^2 + g_+\sigma/l_{sf})}. \end{aligned} \quad (44)$$

(In the second line we took the limits $g_2 \rightarrow 0$, $d \rightarrow 0$, and used $1/l_{sf} \ll q_c \ll q_f$.) This resistance decrease is anticipated on physical grounds since the non-uniform mode allows for an increased transmission of minority electrons that diffuse along the transverse direction — see Fig. 2 and the corresponding discussion in Sec. I.

III. NUMERICAL CALCULATION

The calculations in the preceding section are valid for currents close to the onset of the instability. For currents much larger than the critical current, we need to go beyond perturbation theory to obtain the dynamics. Hereto we numerically solve for the magnetization dynamics and its effect on the resistance of the ferromagnetic layer.

In our numerical analysis, we assume $W_z \ll W_y$ and impose that the magnetization direction $\mathbf{m}(y, z)$ does not depend on z . The remaining two-dimensional problem is replaced by a finite number of one-dimensional problems by substituting the normal-metal spacer and the ferromagnetic layer by N normal metal channels, each attached to a magnet with magnetization direction $\mathbf{m}(n)$, $n = 1, \dots, N$. In order to model a higher-dimensional structure, electrons are allowed to diffuse between the channels, whereas the N magnets interact via an exchange energy. A schematic drawing of this model is shown in Fig. 4.

In this discretized model, the potentials for charge and

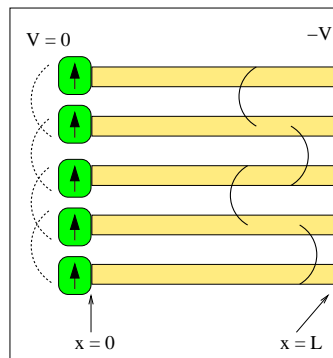


FIG. 4: Schematic drawing of the model solved numerically. The continuous magnet is replaced by N magnets (left), each coupled to a normal-metal wire (right). The wires are coupled via transverse diffusion (shown schematically as solid lines); the magnets are coupled via the exchange interaction (shown schematically as dashed lines).

spin obey the equations

$$\begin{aligned} \partial_x^2 \mu_c(n, x) + \left(\frac{N}{W_y}\right)^2 [\mu_c(n+1, x) + \mu_c(n-1, x) - 2\mu_c(n, x)] &= 0, \\ \partial_x^2 \mu_s(n, x) + \left(\frac{N}{W_y}\right)^2 [\mu_s(n+1, x) + \mu_s(n-1, x) - 2\mu_s(n, x)] &= \frac{\mu_s(n, x)}{l_{sf}^2}. \end{aligned} \quad (45)$$

Equations for the boundary channels, $n = 1$ and $n = N$, are obtained by setting $\mu_{c,s}(0, x) = \mu_{c,s}(1, x)$ and $\mu_{c,s}(N+1, x) = \mu_{c,s}(N, x)$. The general solution of Eq. (45) is of the form

$$\begin{aligned} \mu_c(n, x) &= 2 \sum_{l=0}^{N-1} a_c(l) \cos[l\pi(n+1/2)/N] e^{-q_c(l)x} \\ &\quad + \frac{eIx}{\sigma W_y W_z}, \\ \mu_s(n, x) &= 2 \sum_{l=0}^{N-1} a_s(l) \cos[l\pi(n+1/2)/N] e^{-q_s(l)x}, \end{aligned} \quad (46)$$

with

$$\begin{aligned} q_c(l)^2 &= 4(N/W_y)^2 \sin^2(l\pi/2N), \\ q_s(l)^2 &= l_{sf}^{-2} + 4(N/W_y)^2 \sin^2(l\pi/2N). \end{aligned} \quad (47)$$

The boundary conditions at $x = 0$ (normal-metal-ferromagnet interface) are given by Eq. (3).

The magnetization dynamics is given by the Landau-Lifshitz-Gilbert equation (11), with a discretized exchange torque $\boldsymbol{\tau}_{ex}$,

$$\boldsymbol{\tau}_{ex}(n) = \frac{J\gamma MN^2}{W_y^2} [\mathbf{m}(n+1) + \mathbf{m}(n-1)] \times \mathbf{m}(n), \quad (48)$$

For the anisotropy torque we consider two different cases: The limit of a large applied magnetic field,

$$\boldsymbol{\tau}_{\text{an}} = \frac{k\gamma}{M} \mathbf{e}_3 \times \mathbf{m}(n), \quad (49)$$

as well as the case of no applied field, where we take a simple model for the torque arising from magnetocrystalline and shape anisotropy,

$$\boldsymbol{\tau}_{\text{an}}(n) = -\frac{\gamma}{M} [k_1 m_1(n) \mathbf{e}_1 + k_2 m_2(n) \mathbf{e}_2] \times \mathbf{m}(n). \quad (50)$$

The Landau-Lifshitz-Gilbert equation, together with the boundary conditions at $x = 0$, are sufficient to de-

termine the $4N$ expansion coefficients $a_c(l)$ and $\mathbf{a}_s(l)$, $l = 0, \dots, N-1$, and the time derivative of the magnetization directions $\mathbf{m}(n)$, $n = 1, \dots, N$. Our numerical procedure consists of first expressing $\dot{\mathbf{m}}(n)$ in terms of the potential expansion coefficients $a_c(l)$ and $\mathbf{a}_s(l)$ using the Landau-Lifshitz-Gilbert equation, and then solving for the potential expansion coefficients using the boundary condition at $x = 0$.

For the practical implementation of this scheme, it is useful to define 3×3 matrices \mathcal{M} and $\mathcal{R} = \mathbf{m}\mathbf{m}^T$ such that for any vector \mathbf{v} , $\mathbf{v} \times \mathbf{m} = \mathcal{M}\mathbf{v}$ and $\mathcal{R} - \mathbb{1}_3 = \mathcal{M}^2$. In 3×3 matrix notation, the time derivative of the magnetization vector can be expressed in terms of the potential coefficients as

$$\dot{\mathbf{m}}(n) = \frac{\beta' \mathbb{1}_3 + \alpha'^2 \mathcal{R} / \beta' - \alpha' \mathcal{M}}{\alpha'^2 + \beta'^2} \times \left\{ \mathcal{M}[\boldsymbol{\tau}_{\text{ex}} + \boldsymbol{\tau}_{\text{an}}] + \frac{2\hbar\gamma}{Mde^2} \sum_{l=0}^{N-1} [\mathcal{M}g_1 + g_2 \mathbb{1}_3] \mathcal{M}\mathbf{a}_s(l) \cos[l\pi(n+1/2)/N] \right\}, \quad (51)$$

where $\alpha' = \alpha + \hbar^2\gamma g_1 / (Mde^2)$ and $\beta' = 1 + \hbar^2\gamma g_2 / (Mde^2)$. In turn, the potential coefficients $\mathbf{a}_s(l)$ are obtained from inverting a $4N$ dimensional matrix equation,

$$\sum_{l=0}^{N-1} 2 \cos(l\pi(n+1/2)/N) \begin{bmatrix} 2\sigma q_c(l) + 2g_+ & 2\mathbf{m}^T g_- \\ 2\mathbf{m} g_- & \sigma q_s(l) \mathbb{1}_3 + 4\chi_1 \end{bmatrix} \begin{pmatrix} a_c(l) \\ \mathbf{a}_s(l) \end{pmatrix} = \frac{2eI}{W_y W_z} \begin{pmatrix} g_+ \\ g_- \mathbf{m} \end{pmatrix} + \begin{pmatrix} 0 \\ \boldsymbol{\chi}_2 \end{pmatrix}, \quad (52)$$

where we abbreviated

$$\chi_1(n) = g_- \mathcal{R} - \mathcal{M}(g_1 \mathcal{M} + g_2 \mathbb{1}_3) + \frac{\hbar^2\gamma}{2Mde^2(\alpha'^2 + \beta'^2)} (g_1 \mathcal{M} + g_2 \mathbb{1}_3) [\beta' \mathbb{1}_3 + \alpha'^2 \mathcal{R} / \beta' - \alpha' \mathcal{M}] \mathcal{M}(g_1 \mathcal{M} + g_2 \mathbb{1}_3), \quad (53)$$

$$\boldsymbol{\chi}_2(n) = \frac{2(g_1 \mathcal{M} + g_2 \mathbb{1}_3) \hbar^2\gamma}{Mde^2(\alpha'^2 + \beta'^2)} [\beta' \mathbb{1}_3 + \alpha'^2 \mathcal{R} / \beta' - \alpha' \mathcal{M}] \mathcal{M}[\boldsymbol{\tau}_{\text{ex}}(n) + \boldsymbol{\tau}_{\text{an}}(n)]. \quad (54)$$

We have performed numerical simulations for N ranging between 10 and 20, although all data shown are for $N = 10$ and $N = 11$. We verified that there is no qualitative dependence on the parity of N in our simulations. A small random torque was added at each time step to mimic the effect of a small but finite temperature. (The corresponding temperature obtained from the fluctuation-dissipation theorem was less than a mK.²⁰)

Below we present our results. We first consider the case in which the anisotropy torque is dominated by an applied magnetic field, taking Eq. (49) for the anisotropy torque $\boldsymbol{\tau}_{\text{an}}$. We then consider the case in which there is no applied magnetic field, taking Eq. (50) for $\boldsymbol{\tau}_{\text{an}}$. The latter case is qualitatively different from the former, as it has two stable equilibria for \mathbf{m} ($\mathbf{m} = \mathbf{e}_3$ and $\mathbf{m} = -\mathbf{e}_3$), whereas in the presence of a large applied field the

equilibrium position is at $\mathbf{m} = \mathbf{e}_3$.

A. Large applied magnetic field

For the numerical simulations with a magnetic field, we took values for the various parameters as follows: thickness $d = 0.2$ nm, Width $W_y = 55$ nm, as is appropriate for typical nanopillar experiments,⁷ spin-diffusion length $l_{\text{sf}} = 100$ nm, $\sigma/l_{\text{sf}} = 10^{15} \Omega^{-1} \text{m}^{-2}$, $g_1 = 5.5 \times 10^{14} \Omega^{-1} \text{m}^{-2}$, $g_2 = 0.3 \times 10^{14} \Omega^{-1} \text{m}^{-2}$, $g_{\uparrow} = g_+ + g_- = 4.2 \times 10^{14} \Omega^{-1} \text{m}^{-2}$, $g_{\downarrow} = g_+ - g_- = 3.3 \times 10^{14} \Omega^{-1} \text{m}^{-2}$. The interface conductivities are taken from numerical calculations for a disordered Cu/Co interface,¹⁴ the conductivity σ and the spin relaxation length l_{sf} are consistent with those in Cu. We further

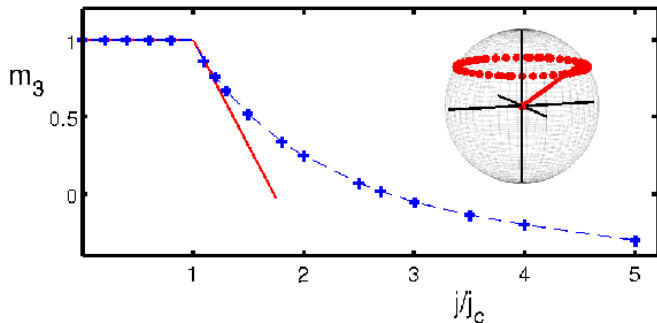


FIG. 5: Main panel shows the magnetization component $m_3(1)$ of the first magnet, as a function of applied current. The solid line is obtained from the perturbation theory result (41), while the dashed line is a guide to the eye. In a large magnetic field, the motion is circular. An example is shown in the inset where $j = 1.5j_c$.

took $\alpha = 0.01$, $\hbar\gamma g_1/Mde^2 = 0.0138$, $j_f = 10^{12}\text{A/m}^2$, $q_f = 10^{-1}\text{nm}^{-1}$ (as is appropriate for Co, see Ref. 41; the magnetic field corresponding to the values of j_f and q_f listed above is of a strength comparable to the intrinsic anisotropy energy). For these parameters, the width of the sample is so small that the spinwave wavenumber q is set by the finite sample width, $q = \pi/W_y$.

For current densities below j_c , no spinwaves are excited. Simulation runs in which the magnetization is tilted away from the easy axis \mathbf{e}_3 show damped precession towards the equilibrium magnetization direction $\mathbf{m} = \mathbf{e}_3$. For current densities above j_c , a spin-wave with wavenumber $q = \pi/W_y$ is excited. Each magnet n in our simulation $n = 1, \dots, N$ shows circular precession around the direction of the applied magnetic field, see Fig. 5, inset. The amplitude of the oscillation increases with current as predicted by the perturbation theory of the preceding section. The 3-component of the magnetization is a constant of the motion and can be monitored to measure the amplitude. Numerical results for m_3 for the magnet $n = 1$ are shown in Fig. 5 as a function of current density, together with a comparison of our numerical results with the perturbative result (41). With a large applied field, the magnetization dynamics remains regular even for current densities much larger than j_c . The effect of the spin-wave instability on the resistance of the ferromagnetic layer is shown in Fig. 6.

B. No applied magnetic field

We have also performed numerical simulations in the absence of an applied magnetic field. Hereto, we choose Eq. (50) for the anisotropy torque, and choose k_1 and k_2 such that $(k_1 - k_2)/(k_1 + k_2) = 0.99$. This form of the anisotropy is appropriate for thin magnetic layers, in which the magnetic anisotropy is predominantly of easy-plane type. The magnitude of the anisotropy energy is set

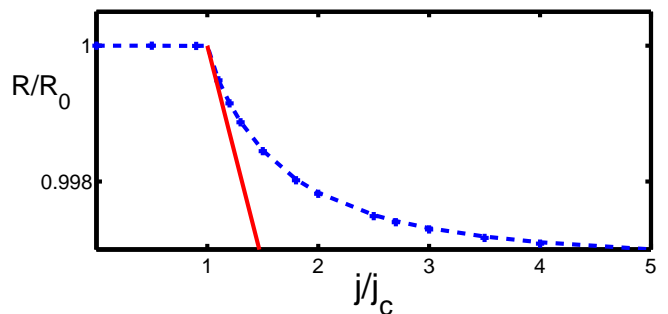


FIG. 6: Resistance of the ferromagnetic layer, as a function of applied current (crosses). The solid line is obtained from the perturbation theory result (44), while the dashed line is a guide to the eye.

by the parameters q_f and j_f , for which we take the same values as in the previous subsection. All other parameters are also taken the same as in the previous subsection.

The magnetization dynamics without applied magnetic field is much richer than the magnetization dynamics at a large magnetic field. The reason is the existence of two stable equilibrium directions if no external magnetic field is applied ($\mathbf{m} = \mathbf{e}_3$ and $-\mathbf{e}_3$). At sufficiently large current densities, the current-induced torque drives the magnetization direction between these two stable directions, leading to a variety of dynamical phases.

For the numerical parameters chosen in our simulation, we observe the following characteristic dynamical modes: For current densities $j_c < j \lesssim 2j_c$ the instability develops with the wavenumber $q = \pi/W_y$. Because the magnetic anisotropy energy used for the simulation has no rotation symmetry around the 3 axis, the magnetization direction $\mathbf{m}(n)$ of each magnet $n = 1, \dots, N$ traces out an ellipse, rather than a circle. We describe the magnetization motion is described using Poincaré sections for the polar angles θ and ϕ for the magnetization. The top right panel in Fig. 7 shows traces that are symmetric about $\phi = \pi$, which have the functional form for \mathbf{m} as predicted by the perturbation theory in the preceding section.

For higher currents with $2j_c \lesssim j \lesssim 2.5j_c$, the reflection symmetry about the easy axis is spontaneously broken, resulting in asymmetric ellipses (upper inset in Fig. 8), which for even higher current densities turn into orbits around the direction perpendicular to the easy axis (lower inset in Fig. 8). A three-dimensional rendering of this regime is shown in Figure 8.

For even larger currents there is a transition into non-periodic modes that cover a significant part of phase space, as shown in Figure 9. Whereas these modes are non-ergodic for lower current densities, they eventually become ergodic and chaotic at high current densities, with Lyapunov exponents increasing with the current density j (data not shown).

In this general case, when the magnetization motion is not just simple circular precession, the spin-wave instability not only leads to a decrease of the dc resistance of

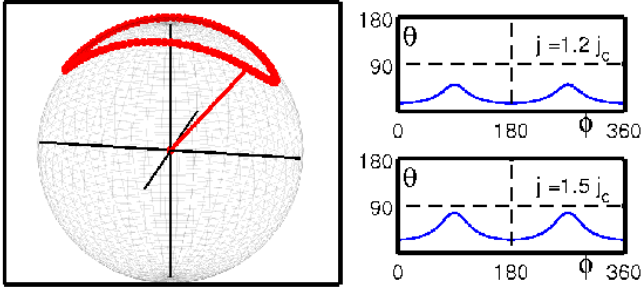


FIG. 7: Typical elliptical trajectory for one of the discrete nanomagnets $\mathbf{m}(n)$ for weak easy axis and strong easy plane anisotropy with $j_c < j < 2j_c$ (left panel). The upper and lower right panels show the corresponding Poincaré sections for $j = 1.2j_c$ and $1.5j_c$ respectively. This regime agrees with the perturbative calculation of Sec. II, where the lowest energy spin-wave mode is excited and increasing the current only changes the amplitude of elliptical oscillation.

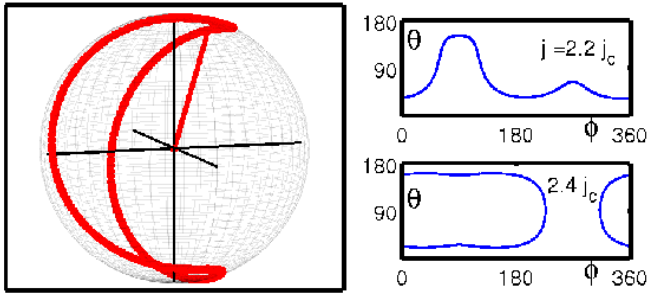


FIG. 8: First manifestations of further dynamical instabilities in the range $2j_c < j < 2.5j_c$. The upper right panel shows a Poincaré section for $j = 2.2j_c$ where the motion is no longer symmetric about the easy axis. The lower right panel shows the motion for $j = 2.4j_c$ where the motion is trapped between the $\pm\hat{e}_3$ easy axes direction. The left panel shows what this motion looks like on the unit sphere.

the ferromagnetic layer, it also causes a fast oscillation of the resistance as shown in the time trace in Figure 10. The right panel in Fig. 10 shows the decrease of the dc resistance up to $j = 2.5j_c$. (No sufficiently accurate numerical results were obtained for larger current density.) Results for the variation of the resistance amplitude and frequency with the applied current density are shown in the left panel for current densities up to $4j_c$. At the parameter values considered in our simulation, the onset of the non-periodic magnetization variations is accompanied by a sharp rise in precession frequency and a decrease of the amplitude of the resistance fluctuations.

IV. CONCLUSION

We have presented a detailed study of the transverse spin-wave instability for a single ferromagnetic layer subject to a large current perpendicular to the layer. Our

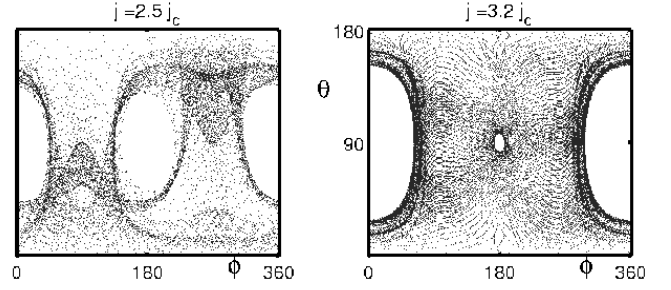


FIG. 9: Poincaré sections for the magnetization direction of one of the magnets at $j = 2.5j_c$ (left) and $j = 3.2j_c$ (right).

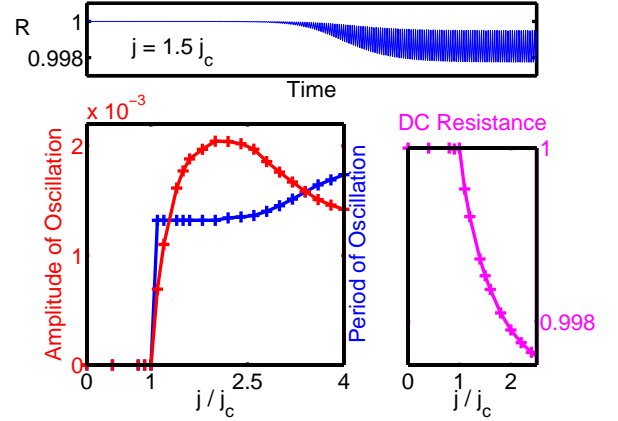


FIG. 10: The upper panel shows the time trace of resistance where the spin-wave instability causes a decrease in the observed resistance. The lower left plot shows how the amplitude and period of the resistance oscillation change with the driving current, while the lower right panel shows the decrease of dc resistance.

calculations have been in the small-amplitude regime, where perturbation theory can be used, and in the large-amplitude regime, where the magnetization dynamics can be solved numerically.

The two main signatures of the spin-wave instability are (1) existence of the instability for one current direction only, and (2) a small reduction in the dc resistance of the ferromagnetic layer. The resistance decrease arises because the existence of a spin wave with large amplitude lowers the spin accumulation in the normal metal adjacent to the ferromagnet. A lower spin accumulation corresponds to a lower resistance (just as a high spin accumulation state of the antiparallel configuration in the standard current-perpendicular-to-plane giant magnetoresistance geometry gives a high resistance state). Both features have been seen in a recent experiment.²⁹

An important question for a dynamical instability is whether or not it is hysteretic. Our calculation has shown that the instability studied here is not, if a large magnetic field is applied. Without applied magnetic field, the nature of the spin wave instability depends on the precise form of the magnetic anisotropy, and both hysteretic and

non-hysteretic behavior can be expected, in principle.

A noteworthy aspect of our calculation is that the spin-transfer torque is calculated self-consistently: the magnitude and direction of the spin-transfer torque depends on the spin accumulation in the normal metal, which, in turn, depends on the precise magnetization profile of the ferromagnet. In doing this, our work connects the the circuit theory for hybrid ferromagnet–normal-metal systems, which has been used extensively to describe the magnet’s effect on spin accumulations in macrospin approximation,¹⁵ and micromagnetic simulations, which, to date, have been restricted to simplified models for the spin-transfer torque. However, our simulations should be considered a proof-of-principle. They lack the spatial resolution and sophistication that full-scale micromagnetic simulations have.

Acknowledgments

We would like to thank A. Kent, I. Krivorotov, B. Özyilmaz, D. Ralph, and Ya. Tserkovnyak for discussions. This work was supported by the Cornell Center for Materials research under NSF grant no. DMR 0079992, the Cornell Center for Nanoscale Systems under NSF grant no. EEC-0117770, by the NSF under grant no. DMR 0334499, and by the Packard Foundation.

APPENDIX

The perturbative calculation of Sec. II focused on the case of a large applied magnetic field because, in that case, theoretical results for the spin wave amplitude do not depend on sample-dependent anisotropy energies. In this appendix we outline the theory for the general case.

For the most general case, one needs a better ansatz for the intrinsic torque $\boldsymbol{\tau}_{\text{an}}$ than Eqs. (14) or (15), as well

as an expression for the current-induced torque that does not rely on rotation symmetry around the easy axis. The general expression for the torque $\boldsymbol{\tau}_{\text{an}}$ is most conveniently derived from the Free energy, $\boldsymbol{\tau}_{\text{an}} = -(\gamma/M)(\partial F/\partial \mathbf{m}) \times \mathbf{m}$. Since we are interested in the mode $\mathbf{m}(\mathbf{q}_c)$ only, we can expand F in powers of $m_1(\mathbf{q}_c)$ and $m_2(\mathbf{q}_c)$, up to fourth order as

$$F(\mathbf{m}) = \frac{1}{2} [k_1 m_1(\mathbf{q}_c)^2 + k_2 m_2(\mathbf{q}_c)^2] + \sum_{j=0}^3 k'_j m_1(\mathbf{q}_c)^j m_2(\mathbf{q}_c)^{3-j} + \sum_{j=0}^4 k''_j m_1(\mathbf{q}_c)^j m_2(\mathbf{q}_c)^{4-j}. \quad (55)$$

The higher-order expansion constants k'_j , $j = 0, 1, 2, 3$, and k''_j , $j = 0, 1, \dots, 4$, are not governed by any special symmetry and therefore likely to be sample specific. (The cubic terms in the expansion of $F(\mathbf{m})$ may be forbidden if there is a reflection symmetry around the easy axis. However, there is no such symmetry in the presence of an applied magnetic field that is not aligned with the one of the sample’s easy or hard axes, so that cubic terms need to be included in a general treatment.) Note that the higher-order torque terms are as important in determining the spin wave amplitude as the higher-order current-induced spin-transfer torque. Unless these coefficients are known independently, a calculation of the spin wave amplitude has no predictive value — that was the reason why the main text addressed the case of a large applied magnetic field.

We now list our general results for the second and third order potentials and third-order spin-transfer torque. The symbols used are defined in Sec. II of the main text. The second-order charge potential expansion coefficients for the normal-metal spacer are

$$a_c^{(2)}(\mathbf{q}) = ej \sum_{\mathbf{q}'} \left\{ \frac{[G_s(0) + G_s(\mathbf{q}) - 2G_s(\mathbf{q}')]D(\mathbf{q}') + 2[G_s(0) - G_s(\mathbf{q}')] [G_s(\mathbf{q}) - G_s(\mathbf{q}')] [g_1 + G_s(\mathbf{q}')] }{D(\mathbf{q}')g_m(0)g_m(\mathbf{q})} \right. \\ \times [m_1(\mathbf{q}')m_1(\mathbf{q} - \mathbf{q}') + m_2(\mathbf{q}')m_2(\mathbf{q} - \mathbf{q}')] \\ \left. - \frac{2g_2[G_s(0) - G_s(\mathbf{q})][G_s(\mathbf{q}) - G_s(\mathbf{q}')] }{D(\mathbf{q}')g_m(0)g_m(\mathbf{q})} [m_1(\mathbf{q}')m_2(\mathbf{q} - \mathbf{q}') - m_2(\mathbf{q}')m_1(\mathbf{q} - \mathbf{q}')] \right\} \\ - \hbar \sum_{\mathbf{q}'} \left\{ \frac{g_2[G_s(\mathbf{q}) - G_s(\mathbf{q}')]G_s(\mathbf{q})}{D(\mathbf{q}')g_m(\mathbf{q})} [m_1(\mathbf{q} - \mathbf{q}')\dot{m}_1(\mathbf{q}') + m_2(\mathbf{q} - \mathbf{q}')\dot{m}_2(\mathbf{q}')] \right. \\ \left. + \frac{[G_s(\mathbf{q}) - G_s(\mathbf{q}')] [D(\mathbf{q}') - G_s(\mathbf{q}')] (g_1 + G_s(\mathbf{q}'))}{D(\mathbf{q}')g_m(\mathbf{q})} [m_1(\mathbf{q} - \mathbf{q}')\dot{m}_2(\mathbf{q}') - m_2(\mathbf{q} - \mathbf{q}')\dot{m}_1(\mathbf{q}')] \right\}. \quad (56)$$

The coefficient $a_c^{(2)}(0)$ determines how the spin wave instability affects the resistance of the ferromagnetic layer, cf. Eq. (44) in the main text. The second order correction to the 3-component of the spin potential is given by the

expansion coefficients

$$\begin{aligned}
\mathbf{a}_{s3}^{(2)}(\mathbf{q}) = & e j \sum_{\mathbf{q}'} \left\{ \frac{1}{2g_m(0)} [m_1(\mathbf{q}')m_1(\mathbf{q} - \mathbf{q}') + m_2(\mathbf{q}')m_2(\mathbf{q} - \mathbf{q}')] \right. \\
& - \frac{1}{D(\mathbf{q}')g_m(0)g_m(\mathbf{q})} [D(\mathbf{q}')(g_+ + 2G_c(\mathbf{q}))(G_s(0) + G_s(\mathbf{q}) - 2G_s(\mathbf{q}')) \\
& \quad - (G_s(0) - G_s(\mathbf{q}'))(g_1 + G_s(\mathbf{q}))(g_m(\mathbf{q}) - 2(g_+ + 2G_c(\mathbf{q}))(G_s(\mathbf{q}) - G_s(\mathbf{q}')))] \\
& \quad \times [m_1(\mathbf{q}')m_1(\mathbf{q} - \mathbf{q}') + m_2(\mathbf{q}')m_2(\mathbf{q} - \mathbf{q}')] \\
& - \frac{g_2[G_s(0) - G_s(\mathbf{q})][2(g_+ + 2G_c(\mathbf{q}))(G_s(\mathbf{q}) - G_s(\mathbf{q}')) - g_m(\mathbf{q})]}{D(\mathbf{q}')g_m(0)g_m(\mathbf{q})} [m_1(\mathbf{q})m_2(\mathbf{q} - \mathbf{q}') - m_2(\mathbf{q})m_1(\mathbf{q} - \mathbf{q}')] \left. \right\} \\
& - \hbar \sum_{\mathbf{q}'} \left\{ \frac{g_2 G_s(\mathbf{q}') [g_m(\mathbf{q}) - 2(g_+ + 2G_c(\mathbf{q}))(G_s(\mathbf{q}) - G_s(\mathbf{q}'))]}{2D(\mathbf{q}')g_m(\mathbf{q})} [m_1(\mathbf{q} - \mathbf{q}')\dot{m}_1(\mathbf{q}') + m_2(\mathbf{q} - \mathbf{q}')\dot{m}_2(\mathbf{q}')] \right. \\
& - \frac{[D(\mathbf{q}') - G_s(\mathbf{q}')(g_1 + G_s(\mathbf{q}'))][g_m(\mathbf{q}) - 2(g_+ + 2G_c(\mathbf{q}))(G_s(\mathbf{q}) - G_s(\mathbf{q}'))]}{2D(\mathbf{q}')g_m(\mathbf{q})} \\
& \left. [m_1(\mathbf{q} - \mathbf{q}')\dot{m}_2(\mathbf{q}') - m_2(\mathbf{q} - \mathbf{q}')\dot{m}_1(\mathbf{q}')] \right\}, \tag{57}
\end{aligned}$$

The very first term describes the effect of a uniform magnetization rotation; the remaining terms are the result of a non-uniform magnetization. There are second-order corrections to the spin potential expansion coefficients a_1 and a_2 that arise from the presence of cubic terms in the anisotropy Free energy. Such cubic terms cause second-order contributions to the time derivatives \dot{m}_1 and \dot{m}_2 , which give a contribution to the second order spin potentials $a^{(2)}$ in the same way as the first-order time contribution to the time derivative affects the first-order spin potentials $a^{(1)}$, see Eq. (21).

Instead of listing the third-order potentials $a^{(3)}$, we describe the corresponding current-induced torque. We specialize to the contributions that are cubic in the magnetization amplitude at wavevector \mathbf{q}_c . The resulting torque has terms proportional to the third-order contributions to the time derivatives of the magnetization. These terms give rise to a renormalized Gilbert damping coefficient and a renormalized gyromagnetic ratio, see Eq. (22). The remaining terms can be written as $2\tilde{\tau}(0) + \tilde{\tau}(2\mathbf{q}_c)$, where (again using two-component spinor notation)

$$\begin{aligned}
\tilde{\tau}^{(3)}(\mathbf{k}) = & \frac{-\hbar\gamma}{2Mde^2 D(\mathbf{q}_c)^2 g_m(0)g_m(\mathbf{k})} \\
& \times \left\{ 2e j g_2 D(\mathbf{q}_c) G_s(\mathbf{q}_c) [G_s(\mathbf{q}_c) - G_s(\mathbf{k})] [g_+ + 2G_c(\mathbf{k})] [G_s(0) - G_s(\mathbf{q}_c)] i\sigma_2 m(\mathbf{q}_c) m^T(\mathbf{q}_c) m(\mathbf{q}_c) \right. \\
& - [g_m(\mathbf{k}) + 2(g_+ + 2G_c(\mathbf{k}))(G_s(\mathbf{q}_c) - G_s(\mathbf{k}))] \\
& \times [-e j [(2G_s(\mathbf{q}_c) - G_s(0) - G_s(\mathbf{k}))D(\mathbf{q}_c) + 2(G_s(0) - G_s(\mathbf{q}_c))(g_1 + G_s(\mathbf{q}_c))(G_s(\mathbf{q}_c) - G_s(\mathbf{k}))] \\
& \quad \times [D(\mathbf{q}_c) - G_s(\mathbf{q}_c)(g_1 + G_s(\mathbf{q}_c))] m(\mathbf{q}_c) m^T(\mathbf{q}_c) m(\mathbf{q}_c) \\
& + e j g_2 G_s(\mathbf{q}_c) [G_s(\mathbf{q}_c) - G_s(\mathbf{k})] [D(\mathbf{q}_c) + 2(G_s(0) - G_s(\mathbf{q}_c))(g_1 + G_s(\mathbf{q}_c))] i\sigma_2 m(\mathbf{q}_c) m^T(\mathbf{q}_c) m(\mathbf{q}_c) \\
& + \hbar g_2 G_s(\mathbf{q}_c) g_m(0) [G_s(\mathbf{q}_c) - G_s(\mathbf{k})] [D(\mathbf{q}_c) - G_s(\mathbf{q}_c)(g_1 + G_s(\mathbf{q}_c))] \dot{m}(\mathbf{q}_c) m^T(\mathbf{q}_c) m(\mathbf{q}_c) \\
& + (\hbar/2) [G_s(\mathbf{q}_c) - G_s(\mathbf{k})] D(\mathbf{q}_c) g_m(0) [D(\mathbf{q}_c) - G_s(\mathbf{q}_c)(2g_1 + G_s(\mathbf{q}_c))] \\
& \quad \times [m(\mathbf{q}_c) m^T(\mathbf{q}_c) i\sigma_2 \dot{m}(\mathbf{q}_c) - i\sigma_2 m(\mathbf{q}_c) m^T(\mathbf{q}_c) \dot{m}(\mathbf{q}_c)] \\
& \left. + (\hbar/2) [G_s(\mathbf{q}_c) - G_s(\mathbf{k})] g_m(0) [(D(\mathbf{q}_c) - G_s(\mathbf{q}_c)(g_1 + G_s(\mathbf{q}_c)))^2 - (g_2 G_s(\mathbf{q}_c))^2] i\sigma_2 \dot{m}(\mathbf{q}_c) m^T(\mathbf{q}_c) m(\mathbf{q}_c) \right\}. \tag{58}
\end{aligned}$$

Once the perturbative expansions for the anisotropy torque and the current-induced spin-transfer torque are

known, the Landau-Lifshitz-Gilbert equation can be solved for the magnetization dynamics.

¹ J. C. Slonczewski, J. Magn. Magn. Mater. **159**, 1 (1996).

² L. Berger, Phys. Rev. B **54**, 9353 (1996).

³ M. Tsoi, A. G. M. Jansen, J. Bass, W.-C. Chiang, M. Seck,

V. Tsoi, and P. Wyder, Phys. Rev. Lett. **80**, 4281 (1998).

⁴ J. Z. Sun, J. Magn. Magn. Mater. **202**, 157 (1999).

⁵ J.-E. Wegrowe, D. Kelly, Y. Jaccard, P. Guittienne, and

- J.-P. Ansermet, *Europhys. Lett.* **45**, 626 (1999).
- ⁶ E. Myers, D. Ralph, J. Katine, R. Louie, and R. Buhrman, *Science* **285**, 867 (1999).
 - ⁷ J. A. Katine, F. J. Albert, R. A. Buhrman, E. B. Myers, and D. C. Ralph, *Phys. Rev. Lett.* **84**, 3149 (2000).
 - ⁸ S. I. Kiselev, J. C. Sankey, I. N. Krivorotov, N. C. Emley, R. J. Schoelkopf, and R. A. Buhrman, *Nature* **425**, 380 (2003).
 - ⁹ S. I. Kiselev, J. C. Sankey, I. N. Krivorotov, N. C. Emley, M. Rinkoski, C. Perez, R. A. Buhrman, and D. C. Ralph, *Phys. Rev. Lett.* **93**, 036601 (2004).
 - ¹⁰ W. H. Rippard, M. R. Pufall, S. Kaka, S. E. Russek, and T. J. Silva, *Phys. Rev. Lett.* **92**, 027201 (2004).
 - ¹¹ I. N. Krivorotov, N. C. Emley, A. G. F. Garcia, J. C. Sankey, S. I. Kiselev, D. C. Ralph, and R. A. Buhrman, *Phys. Rev. Lett.* **93**, 166603 (2004).
 - ¹² X. Waintal, E. Myers, P. Brouwer, and D. Ralph, *Phys. Rev. B* **62**, 12317 (2000).
 - ¹³ M. D. Stiles and A. Zangwill, *Phys. Rev. B* **66**, 014407 (2002).
 - ¹⁴ K. Xia, P. J. Kelly, G. E. W. Bauer, A. Brataas, and I. Turek, *Phys. Rev. B* **65**, 220401 (2002).
 - ¹⁵ Y. Tserkovnyak, A. Brataas, G. E. W. Bauer, and B. I. Halperin, *cond-mat/0409242* (2004).
 - ¹⁶ J. Z. Sun, *Phys. Rev. B* **62**, 570 (2000).
 - ¹⁷ Y. B. Bazaliy, B. A. Jones, and S.-C. Zhang, *Phys. Rev. B* **69**, 094421 (2004).
 - ¹⁸ Z. Li and S. Zhang, *Phys. Rev. B* **69**, 134416 (2004).
 - ¹⁹ J. Xiao, A. Zangwill, and M. D. Stiles, *cond-mat/0504142* (2005).
 - ²⁰ D. Apalkov and P. Visscher, *cond-mat/0405305* (2004).
 - ²¹ A. Kovalev, G. Bauer, and A. Brataas, *cond-mat/0504705* (2005).
 - ²² Z. Li and S. Zhang, *Phys. Rev. B* **68**, 024404 (2003).
 - ²³ D. Berkov and N. Gorn, *Phys. Rev. B* **71**, 052403 (2005).
 - ²⁴ L. Torres, L. Lopez-Diaz, E. Martinez, M. Carpentieri, and G. Finocchio, *J. Magn. Mag. Mater.* **286**, 381 (2005).
 - ²⁵ D. Berkov and N. Gorn, *cond-mat/0503754* (2005).
 - ²⁶ A. Brataas, Y. V. Nazarov, and G. E. W. Bauer, *Phys. Rev. Lett.* **84**, 2481 (2000).
 - ²⁷ Y. Tserkovnyak, A. Brataas, and G. E. W. Bauer, *Phys. Rev. Lett.* **88**, 117601 (2002).
 - ²⁸ M. L. Polianski and P. W. Brouwer, *Phys. Rev. Lett.* **92**, 026602 (2004).
 - ²⁹ B. Özyilmaz, A. D. Kent, J. Z. Sun, M. J. Rooks, R. H. Koch, *Phys. Rev. Lett.* **93**, 176604 (2004).
 - ³⁰ Y. Ji, C. L. Chien, and M. D. Stiles, *Phys. Rev. Lett.* **90**, 106601 (2003).
 - ³¹ M. D. Stiles, J. Xiao, and A. Zangwill, *Phys. Rev. B* **69**, 054408 (2004).
 - ³² B. Özyilmaz, A. D. Kent, M. J. Rooks, and J. Z. Sun, *Phys. Rev. B* **71**, 140403 (2005).
 - ³³ S. Urazhdin, *Phys. Rev. B* **69**, 134430 (2004).
 - ³⁴ A. Brataas, Y. Tserkovnyak, and G. Bauer, *cond-mat/0501672* (2005).
 - ³⁵ A. Slavin and P. Kabos, *IEEE Trans. Mag.* **41**, 1264 (2005).
 - ³⁶ T. Y. Chen, Y. Ji, C. L. Chien, and M. D. Stiles, *Phys. Rev. Lett.* **93**, 026601 (2004).
 - ³⁷ M. D. Stiles, *J. Appl. Phys.* **79**, 5805 (1996).
 - ³⁸ E. M. Lifschitz and L. P. Pitaevskii, *Statistical Physics, part 2* (Pergamon, 1980).
 - ³⁹ T. L. Gilbert, *IEEE Trans. Mag.* **40**, 3443 (2004).
 - ⁴⁰ Ya. B. Bazaliy, B. A. Jones, and S.-C. Zhang, *Phys. Rev. B* **57**, 3213 (1998).
 - ⁴¹ E. P. Wohlfahrt, in *Ferromagnetic Materials*, edited by E. P. Wohlfahrt (North-Holland, 1980), vol. 1.